Postprint of: Siuzdak K., Ficek M., Sobaszek M., Ryl J., Gnyba M., Niedziałkowski P., Malinowska N., Karczewski J., Bogdanowicz R., Boron-Enhanced Growth of Micron-Scale Carbon-Based Nanowalls: A Route toward High Rates of Electrochemical Biosensing, ACS Applied Materials & Interfaces, Vol. 9, iss. 15 (2017), pp.12982–12992

Boron enhanced growth of micron-length carbon based nanowalls: A route towards high rates electrochemical biosensing

Katarzyna Siuzdak[1], *Mateusz Ficek*[2], *Michał Sobaszek*[2], *Jacek Ryl*[3], *Marcin Gnyba*[2], *Paweł Niedziałkowski*[4], *Natalia. Malinowska*[4], *Jakub Karczewski*[5] *and Robert Bogdanowicz*[2]*

[1] Centre for Plasma and Laser Engineering, The Szewalski Institute of Fluid-Flow Machinery, Polish Academy of Sciences, 14 Fiszera St., 80-231 Gdansk, Poland

[2] Department of Metrology and Optoelectronics, Faculty of Electronics, Telecommunications and Informatics, Gdansk University of Technology, 11/12 G. Narutowicza St., 80-233 Gdansk, Poland

[3] Department of Electrochemistry, Corrosion and Materials Engineering, Faculty of Chemistry, Gdansk University of Technology, 11/12 Narutowicza St., 80-233 Gdansk, Poland

[4] Department of Analytical Chemistry, Faculty of Chemistry, University of Gdansk, 63 Wita Stwosza St., 80-952 Gdansk, Poland

[5] Faculty of Applied Physics and Mathematics, Gdansk University of Technology, 11/12 G. Narutowicza St., 80-233 Gdansk, Poland

Keywords: Boron-doped Carbon Nanowalls, Cyclic Voltammetry, Electrochemical Impedance Spectroscopy, Differential Pulse Voltammetry, DNA Purine Bases

***Corresponding author:** E-mail: rbogdan@eti.pg.gda.pl (Robert Bogdanowicz); Tel.: +48-58-347-15-03; Fax: +48 58-347-18-48

ABSTRACT. In this study we have demonstrated the fabrication of novel material called boron-doped carbon nanowalls (B:CNW) which is characterized by remarkable electrochemical properties like high standard rate constant k°, low peak to peak separation value (ΔE) for oxidation and reduction processes of $[Fe(CN)_6]^{3-/4-}$ redox system and low surface resistivity. The B:CNW samples were deposited by the microwave plasma assisted chemical vapor deposition (CVD) using a gas mixture of H_2:CH_4:B_2H_6 and N_2. Growth results in sharp edge, flat and long carbon nanowalls rich in sp^2 as well as sp^3 hybridized phases. The achieved high values of $k^o = 1.1\times10^{-2}$ cm/s and ΔE as 85 mV are much lower in comparison to the glassy carbon or undoped carbon nanowalls. The enhanced electrochemical performance of B:CNWs electrode applied for the simultaneous detection of DNA purine bases: adenine and guanine. Both separated oxidation peaks for independent determination of guanine and adenine were observed by means of cyclic voltammetry or differential pulse voltammetry. It is worth noting that determined sensitivities and current densities were about one order of magnitude higher than those registered by other electrodes.

1. Introduction

Nowadays, carbon-based materials have a great interest for the scientific and industry community, especially in the sensors, biosensors and electronics area[1]. The most common carbon nanostructures are carbon nanotubes[2], diamond films[3] and graphene[4]. On the other hand, there are carbon nanoflakes[5], nanosheets[6], and carbon nanowalls (CNW).[7] Typically, carbon nanowalls can be described as planar graphene sheets grown vertically to the substrate. Wu *et al.*[7] reported the fabrication of CNW on catalyzed substrates using microwave plasma assisted

CVD. Hiramatsu *et al.*[8] fabricated vertically aligned CNW using coupled radio-frequency and plasma-enhanced CVD. The carbon nanowall sample used for the electrochemical measurement are fabricated using C_2F_6/H_2 or CH_4/H_2 gas sources[9], respectively. Recently, Zhu *et al.* reported B/N-doped carbon nanotube/carbon nanosheets hybrids as the high performance supercapacitor electrode and lithium ion battery anode[10]. To date, only Lu *et al.* have studied catalyst-free vertically aligned boron doped carbon nanowalls but as a potential electron emitting material[11]. However, literature shows only typical CNW exposing semicircular or cauliflower shaped nanoflake morphology[12].

In this study, we have demonstrated for the first time the fabrication of novel material called boron-doped carbon nanowalls (B:CNW) which is characterized by remarkable electrochemical properties like high standard rate constant k°, low peak to peak separation value (ΔE) for the oxidation and reduction processes of $[Fe(CN)_6]^{3-/4-}$ redox system and ultra-low charge transfer resistivity. Boron doping of carbon nanowalls induces the unique effect of enhanced electrochemical performance and improved charge transfer never reported before in literature. Furthermore, a similar boron doping effect could be achieved potentially in other nanowalls materials fabricated by electrodeposition[13], sputtering or RF plasma CVD[8].

The B:CNW samples were deposited by the microwave plasma assisted CVD using a gas mixture consisting of H_2, CH_4, B_2H_6 and N_2. Growth results in sharp edged, flat and long carbon nanowalls rich in sp^2 as well as sp^3 hybridized phases. That novel electrode material results in competitive electrochemical properties when compared with glassy carbon (GC) or previously reported undoped nanowalls[14] or is comparable to that found for functionalized CNW.[15] The detailed properties of B:CNW were delivered using X-ray photoelectron spectroscopy, SEM analysis, Raman spectroscopy and different electrochemical techniques.

Moreover, the simultaneous determination of guanine (G) and adenine (A) or their ratio in DNA was delivered as an example of very important analytical medium[16]. The detection and

quantification of DNA is usually based on electrochemical activity of adenine and guanine. The electrooxidation of adenine and guanine on the bare conventional electrode surfaces give many difficulties due to slow electron transfer kinetics, high positive oxidation potentials often interfered by oxygen evolution, adsorption resulting in the formation of passivation layer as well as large background currents[17]. Due to this fact, many modifications of the electrode have successfully been developed for the detection of DNA bases. The graphene[18], graphene-Nafion composite film modified glassy carbon electrode was used for simultaneous determination of adenine and guanine[19]. The differential pulse voltammetry (DPV) and cyclic voltammetry (CV) were successfully utilized to study the oxidation process of DNA purine bases: adenine and guanine in one solution at physiological pH at the bare, unmodified B:CNW electrode.

2. Results and Discussion

2.1. Morphology and structure of B:CNWs

High resolution scanning microscopy was applied for investigation of surface morphology of B:CNW, e.g. length distribution and height. As it can be seen in **Figure 1A**, the B:CNW can be graded in three major groups depending on wall length. The distribution of nanowalls length is 65%, 25% and 10% for walls longer than 1, 2 and 3 μm, respectively. Previous reports show just short and maze-like CNW[7,20]. Furthermore, **Figure 1B** shows surface profile and the dark blue and orange colors correspond to bottom (substrate) and top edges of B:CNW, respectively. The specific agglomerates of carbon clusters cover the sides of flat carbon walls (attn. marked in **Figure 1B** in cyan color). Moreover, growth of these clusters can be explained by forming nanocrystalline or ultrananocrystalline diamond structures[21] which can be responsible for enhanced charge transfer. The dense polycrystalline structure of B:CNW could facilitate the intercalation of ions into the nanowalls[22], while the short diffusional distance in and out leads

to EDLC devices with higher rates of charge and discharge as revealed similarly in MoS_2[23] or NiO[24] nanosheets.

The height of B:CNW is equal to 3.3 μm after the 6 h deposition process (**Figure 1C**) with carbon clusters of up to half the height of B:CNW which can be observed in the cross-section or 3D reconstruction (see **Figure 1CD**). Hence, it is clearly seen that the top edges of the wall are sharp.

The carbon nanowall growth mechanism involves joint chemistry of many species, not only limited to CN^-, H_yCNH_x, BH^-_x and CH^+_x radicals. The H_yCNH_x are one of the main products of reactions involving H/C/N compounds in plasma. H_yCNH_x species undergo further dissociation to CN^- or CNH^- by thermal decomposition at the heated substrate stage participating in fast H-shifting reactions. The simple molecular geometry and higher electron−ion recombination rates of H_yCNH_x species could be responsible for the directional growth of carbon nanowalls.
First, the nanodiamond seeds support efficient diamond nucleation, preferring sp^3 rich structure growth. The proposed growth mechanism of novel boron-doped nanowalls is as follows: (i) adsorption of a CN^- radicals with its carbon end down due to the lowest bond energy 389 eV; (ii) reactive H radicals lead to a breaking of the weaker bonds creating dangling carbon bonding[25], (iii) attachment of a CH_x radicals or C_2 dimers to the CN^- and independently to the other dangling bonds at the surface; (iv) parallel attachment of BH_x radicals which are responsible for enhanced electrochemical performance and developed morphology; (v) bridging of these adsorbates; (vi) replacing carbon and CN^- radicals with CH_x or BH_x radicals[26], because they are located at the grain boundaries or the top edges of nanowalls. Nitrogen shows just minor concentration in the samples as revealed by XPS (0.4% for 5% N_2 in the plasma).

The very recent study[27] of diamond growth in the H/C/H shows that the N-containing species can be considered as potentially reactive at the growing diamond surface, while these N-induced effects are not the one factor in a multiparameter growth mechanism, so that the

result of adding N_2 to the process mixture also depends on the substrate condition and its temperature during growth. To summarize, the basic understanding of nanowall growth has still not been revealed and needs more investigation. The chance for that gives wide pseudo-potential, density functional theory (DFT) studies.

The previously reported carbon nanowalls, nanosheets or nano-needles growth were attributed only to CN molecules[28]. The films' morphology, shown in the SEM microimages (**see Figure 1**), implies that the nano-diamond grows anisotropically in the N_2/CH_4 plasma. Next, Sankaran *et al.*[29] reported that the growth rates along the longitudinal and circumferential directions vary considerably from the needle-like ultrananocrystalline diamond films grown in in-plane temperatures higher that 700^{o}C that lead to acicular grains.

In that study, the authors suggest that for developed morphology and large size of nanowalls mainly BH_x radicals are responsible. The initial growth of the vertically aligned nanowalls is driven by CN molecules, which favors the formation of edge-N species most rather than the graphitic/quaternary N formation[30]. This fact causes the slow growth rates along the strongly bonded planes of expanding carbon sheets and fast ones along the weakly bonded stacking direction containing CN structures. Next, BH_x replaces part of CN molecules at the edges [e.g. (100)] and additionally causes re-nucleation expanding length of nanowalls as already reported for diamond structure[31].

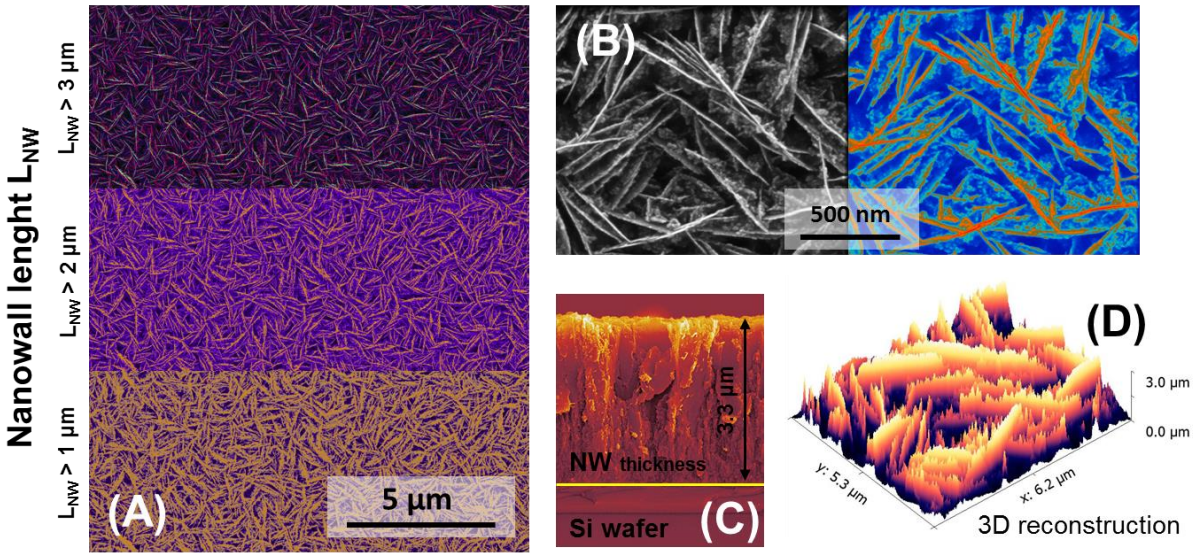

Figure 1. Top-view HR-SEM images of B:CNW: (A) nanowalls length distribution, (B) top-view at higher magnification with corresponding nanowalls pattern, (C) Cross-sectional micro-image, and (D) 3D reconstruction of surface morphology.

Raman spectra of the B:CNW film were collected at two different spots on the sample and respective microscopic images are shown in **Figure 2**. Two main bands at about 1341-1344 cm^{-1} and 1583-1587 cm^{-1} are assigned to *D* band and *G* band respectively [12]. The Raman peaks of "D" and "G" bands show relatively narrow FWHMs of 129 cm^{-1} and 62 cm^{-1} respectively. Those values indicate the crystalline character of nanowalls since they are comparable with highly oriented multiwalled carbon nanotubes[32] or doubled when compared with undoped carbon nanowalls[33]. Moreover, there are two other weak bands in this region. The first one at about 1100-1200 cm^{-1} can be assigned to sp^3 nanocrystalline carbon (*T* band), while the wider bands: the *D* band and *G* band have numerous assignments, e.g. C=C chains (similar to polyacetylene). Estimated I(D)/I(G) ratio was equal to 3.17, while sp^3/sp^2 ratio is 0.67. Comparable values were obtained for hydrogenated CVD graphene films [34] or in defected graphene with average distance between defects of tens of nanometers[35].

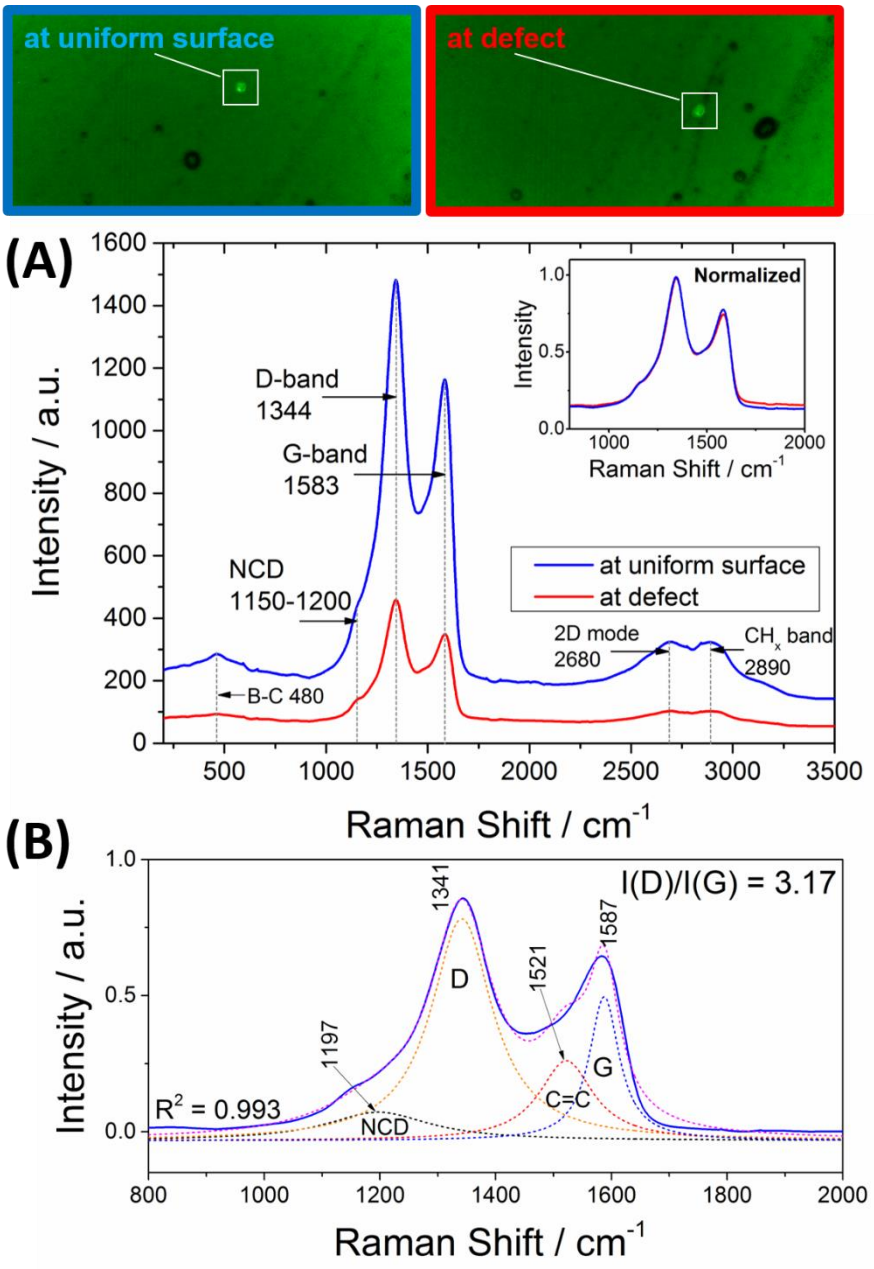

Figure 2. Raman spectra and microscopic images of B:CNW sample collected in two places on the sample (A). Decomposition of the Raman spectra (B).

Furthermore, the band at 2680 cm^{-1} is a *2D* band, while the band at 2890 cm^{-1} can be assigned to C-H stretching vibration. Presence of *T* band as well as *D* and *G* bands confirms that the films contain both C-C sp^3 and C-C sp^2 phase. The achieved results are in agreement with XPS revealed composition. High hydrogenation of B:CNW is supported by pronounced 2890 cm^{-1}

Raman band. Normalized Raman spectra recorded in various spot at the B:CNW are similar with each other. It suggests that the deposited films have homogenous molecular composition and that type of defect refers rather to the various thickness of the structure.

The XPS study of investigated B:CNW is presented in the **Figure 3**. Four components were used during deconvolution of high-resolution XPS spectra acquired in the energy range of C1s. Most notable components are located at binding energy (BE) of 285.1 eV and 284.4 eV and correspond to C-C sp^3 and C-C sp^2, respectively. The third component is a complex peak located at 286.7 eV. It should be connected to both C-O and C=N bonds, which are overlapping each other hindering more detailed analysis. Its shift is in good agreement with other, similar studies[36]. The last peak of C1s deconvolution is positioned at 283.1 eV. This peak has been attributed to the presence of distorted diamond related to the vacancies of hydrogen atoms close to boron atoms. Amongst others, this effect was considered as a consequence of electrode aging under the deep anodic overpotential treatment[37]. Other explanations should also be considered as allocation of this XPS feature is difficult to determine in such a complex system. J.T. Titantah and D. Lamoen[38] investigated amorphous carbon nitride system and drew a conclusion that it may result from two-coordinated carbon atoms in the system while Z.M. Ren *et al.* recognized it to reflect the existence of nanocrystallites of graphite[39]. The sp^3/sp^2 ratio of 0.34 computed form during XPS analysis corroborate with similar measurement done by Raman spectroscopy (0.67), while the difference comes mainly from various depth penetration of both methods. Two peaks contributed during deconvolution of O1s spectra. The main component at 533.0 eV represents C-OC and C-OH while the secondary component, located at 531.6 eV is often ascribed to -OH radicals and C=O bonds. B1s spectrum shows only one component, located at BE of 187.6 eV[40]. Its share in the investigated sample is around 1.3%, as to be expected. Unlike boron, it should be noted that nitrogen is very weakly incorporated into the structure of

nanowalls. Contribution of N1s in the analyzed sample is 0.4% despite the fact that in the gas phase there was 180k ppm [N]/[C] ratio. The low incorporation of nitrogen can be explained by intensive nitrogen removal from surface during growth process by ionized hydrogen species[21,41].

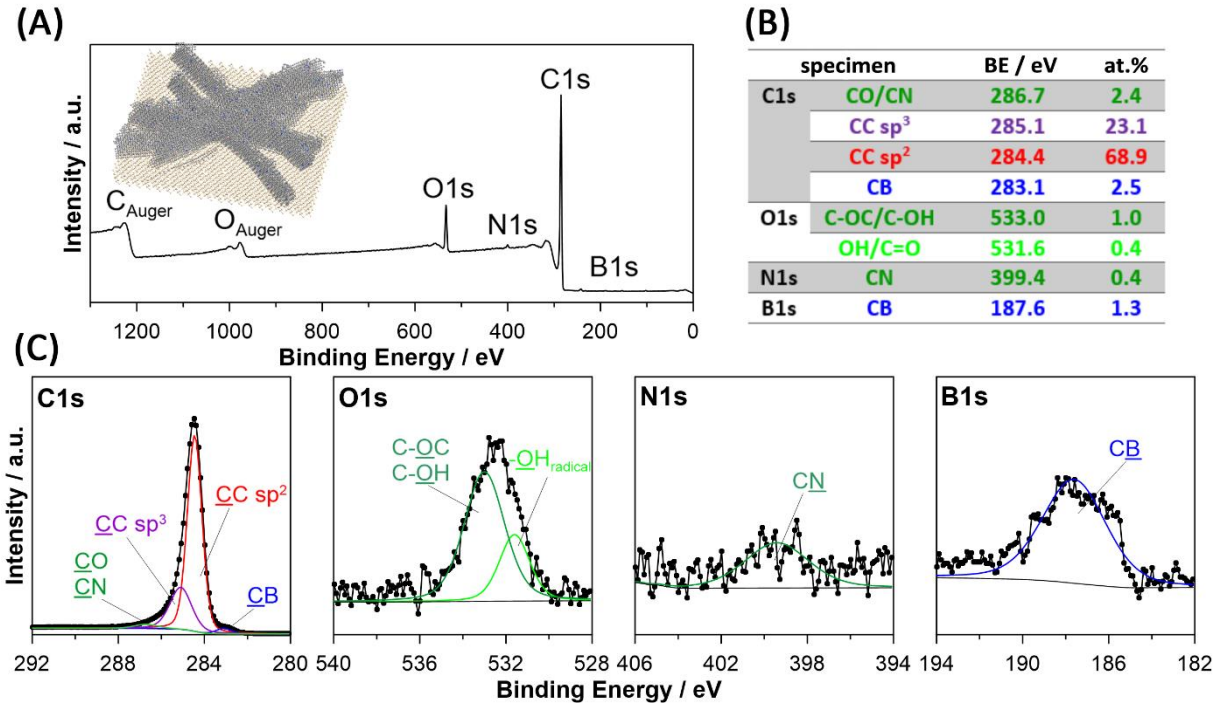

	specimen	BE / eV	at.%
C1s	CO/CN	286.7	2.4
	CC sp^3	285.1	23.1
	CC sp^2	284.4	68.9
	CB	283.1	2.5
O1s	C-OC/C-OH	533.0	1.0
	OH/C=O	531.6	0.4
N1s	CN	399.4	0.4
B1s	CB	187.6	1.3

Figure 3. XPS survey (A), atomic composition analysis (B), high-resolution XPS spectra (C) in energy range of C1s, O1s, N1s and B1s, acquired for B:CNW samples with peaks used during deconvolution and chemical analysis.

2.2. Electrochemical performance of carbon nanowalls

The electrochemical performance of B:CNW and reference samples: CNW and GC has been firstly investigated by cyclic voltammetry measurements in a neutral aqueous solution of 0.5 M K_2SO_4. As it is shown in **Figure 4**, from -1.7 V up to +1.2 V *vs*. Ag/AgCl/3 M KCl, a B:CNW sample exhibit only capacitive behavior resulting from the charge of electrochemical double-layer on the contrary to CNW, where the irreversible oxidation (+0.83 V) and reduction peaks (-0.50 V) significantly narrows the electrochemical potential window. Above this range,

the current increases which is related with decomposition of electrolyte. This range is similar to those observed for glassy carbon electrode, but B:CNW material exhibit higher values of current density related with double layer capacitance that will be later on studied by EIS technique. The B:CNT activity is analogous to that reported for high-quality boron-doped diamond films[15], but simultaneously it is much higher comparing to CNW synthesized by Hassan *et al.*[42] and Kriventko *et al.*[20]. Importantly, within the determined potential window no Faradaic reaction was observed as it was found for other CNW materials contaminated by surface redox active species[43].

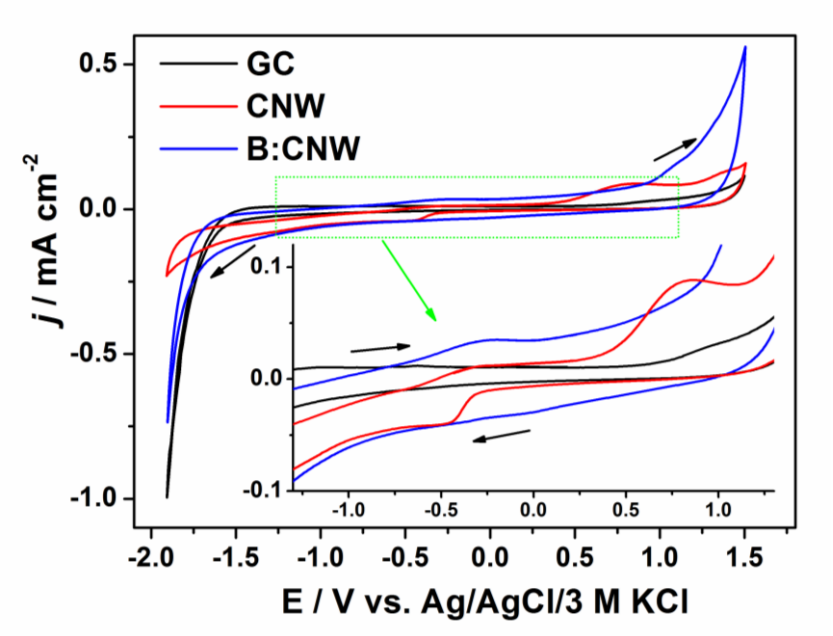

Figure 4. The cyclic voltammetry curves registered for GC, CNW and B:CNW samples in 0.5 M K_2SO_4 (v = 50 mVs^{-1}).

Afterwards, all samples were transferred into the $K_3Fe(CN)_6$ solution and the clear anodic and cathodic peaks assigned to the oxidation and reduction processes of $[Fe(CN)_6]^{3-/4-}$ redox system, respectively were observed (see **Figure 5**).

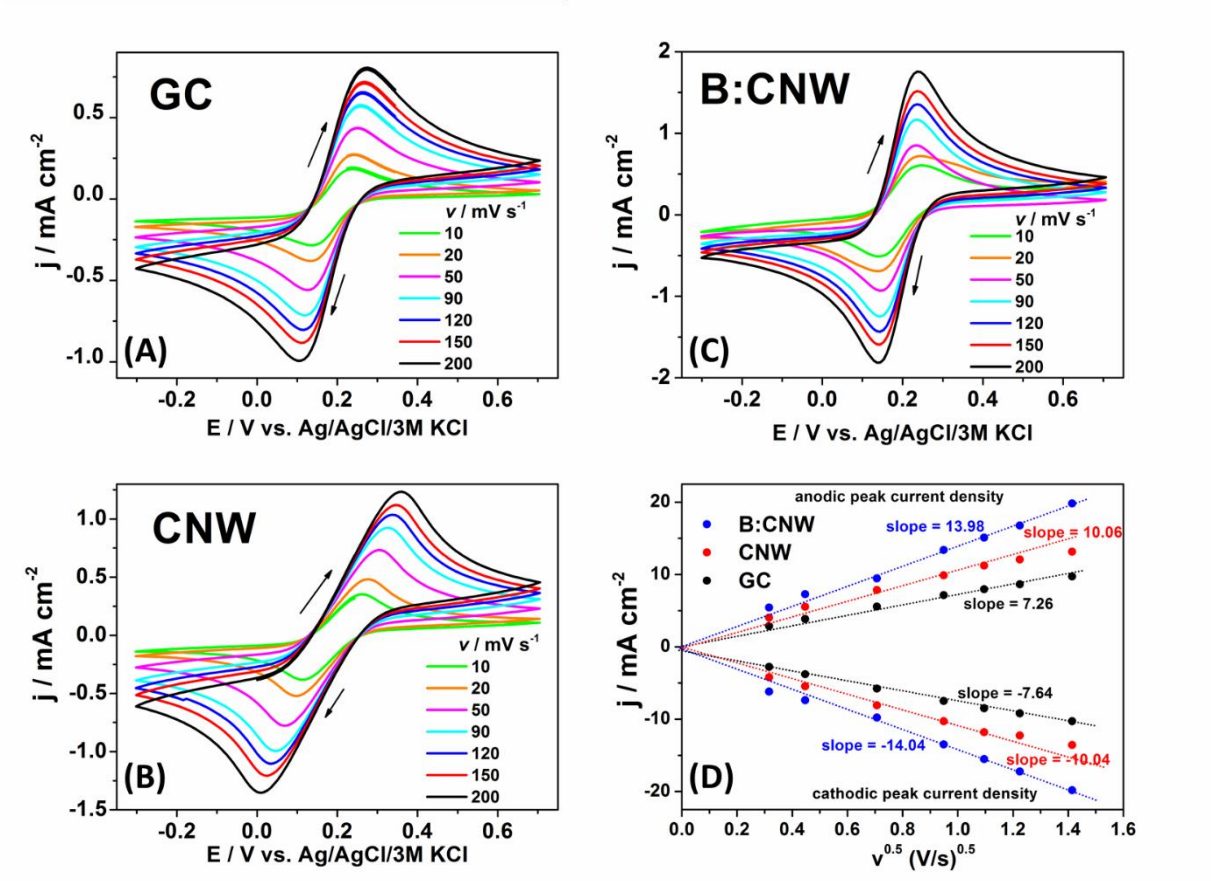

Figure 5. The cyclic voltammetry curves registered for in (A) GC, (B) CNW, (C) B:CNW electrodes immersed in 5 mM $K_3Fe(CN)_6$ + 0.5 M K_2SO_4. (D) Plot of peak current density *vs.* scan rate obtained on the basis of (A-C) CV sets.

Table 1. The values of oxidation (E_{ox}) and reduction potentials (E_{red}) of $[Fe(CN)_6]^{3-/4-}$ redox reaction together with the separation peak value (ΔE).

SAMPLE	EOX / MV	ERED / MV	ΔE / MV
B:CNW	231	146	85
CNW	304	69	235
GC	250	125	125

Among all tested materials, the lowest peak to peak separation value was found for B:CNW and equals 85 mV that is higher only by 26 mV comparing to 59 mV known as an expected value for a Nernstian one-electron reaction (see **Table 1**). As it will be shown later on,

electrolyte resistance is very low, small ΔE value indicates good attachment of B:CNW to the silicon substrate, may result from a high level of surface cleanliness and low surface oxide coverage. Thus, slight peak splitting allows us to describe synthesized B:CNW as material possessing desirable surface structure and electronic properties that support rapid electron transfer for ferricyanide/ferrocyanide redox system. According to CV curves observed in **Figure 5**, an increase in sweeping rate promotes growth of current peak intensity in cathodic and anodic reaction, as well. For $[Fe(CN)_6]^{3-/4-}$ system, the linear dependence of cathodic j_c and anodic j_c current density peaks on the square root of the scan rate passing through zero is observed (see **Figure 5D**).

The symmetry of anodic and cathodic relation indicates that the electron transfer is nearly reversible[20] and the surface of all tested electrode materials is under diffusion-control as it was also exhibited by the relation between the logarithm of anodic and cathodic peak current densities versus the logarithm of the scan rate (see Figure S2). The slopes values equal to ca. 0.44 which is near the theoretical value of 0.5 for a purely diffusion controlled process[44]. Thus, the reaction rate depends only on the supply of redox active species to the electrode surface that is determined by Fick's law. Similar behavior is found for other carbon-like electrode materials, such as graphene, BDD or highly oriented carbon nanowalls.[20,45,46] According to the Randles-Sevcik, equation describing relation between peak current and the $v^{1/2}$: $I_p = (2.69\times10^5 A_{eff} D^{1/2} n^{3/2} C)v^{1/2}$ and on the assumption that the diffusion to the electrode is one-dimensional, an approximate value of electroactive surface area A_{eff} could be estimated[47]. Because both peaks currents are proportional to the square root of the scan rate and D[48], n and C could be regarded as a constant parameters, the effective surface area was found to be equal to 0.45 cm^2, 0.33 cm^2 and 0.06 cm^2 for B:CNW, CNW and GC, respectively**.** Thus, A_{eff} for B:CNW is almost 3.6 times higher comparing to the geometric electrode area that provided a conclusive evidence of the 3D-porous structure of investigated electrode[49] (see **Figure 1D**). It

indicates also that not only surface edges but also side nanowalls planes of the sample could have impact on electrochemical processes and such material can be employed as an ultrasensitive electrode due to its large active surface area[50].

In order to quantify the electronic and ionic conductivities, as well as the diffusive behavior, electrochemical impedance spectroscopy data (EIS) were collected in the range from 20 kHz down to 0.1 Hz. The Nyquist representations of impedance spectra obtained at the formal potential of redox reaction for B:CNW and other electrodes: pure CNW, GC for comparison are shown in **Figure 6.**

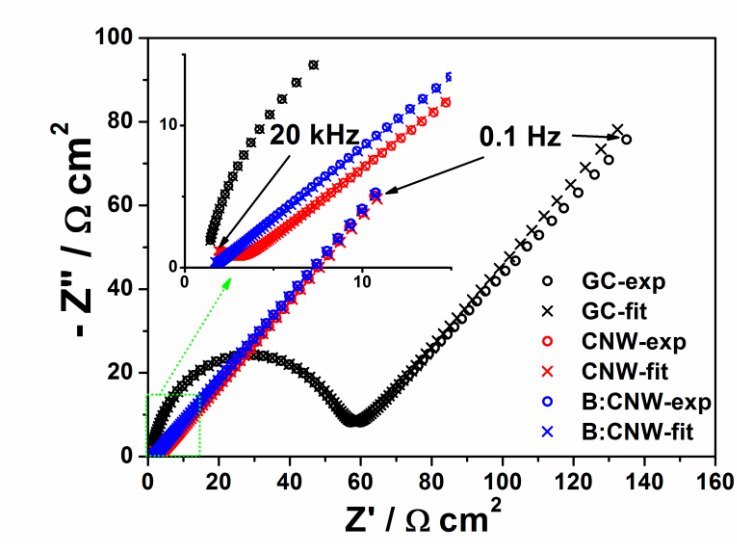

Figure 6. The impedance spectra registered (exp) and fitted (fit) for B:CNW, CNW and GC electrode immersed in 5 mM $K_3Fe(CN)_6$ + 0.5 M K_2SO_4, at the formal potential of redox reaction.

In general, EIS spectra are composed of two parts: high frequency arc and low-frequency straight line with 45° slope. Registered spectra were analyzed on the basis of electric equivalent circuit (*EEQC*) known in literature as Randles circuit: $R_e(CPER_{ct}W)$[51,52]. The fitting procedure gives normalized fitting errors on the level of 4×10^{-5}. The ohmic resistance R_e element in the high frequency regime represents electrolyte resistance and for all materials equals c.a. 1.1

Ω cm^2. The Z_W element that is in the range of 48.9 - 55.9 Ω s$^{-0.5}$, called Warburg impedance, describes mass transport impedance and is assigned to the diffusion of charged species from the bulk of electrolyte to the interface and through the interface layer. The values of remaining elements: R_{ct}, Q parameter of *CPE*, and *W* are collected in **Table 2.**

Table 2. The value of charge transfer resistance and space charge capacitance obtained on the basis of fitting procedure.

Element	B:CNW	CNW	GC
R_{ct} / Ω cm^2	4.7	14.1	53.3
Q / Ω^{-1} cm^{-2} s^n	1.6×10^{-4}	2.9×10^{-5}	9.9×10^{-6}
W / Ω s$^{-0.5}$	49.9	49.5	55.9

The R_{ct} arising in the high frequency regime represents charge transfer resistance whereas *CPE* is assigned to the double layer capacitance. According to **Table 2**, the lowest value of R_{ct} is exhibited by B:CNW and simultaneously it differs significantly from other carbon based electrode materials: the nitrogen modified diamond nanowire electrode (322 kΩ cm^2)[52], sample of boron doped diamond pretreated in sulphuric acid (210-240 Ω)[53], reduced BDD pretreated in acetate buffer or sulphuric acid (2.7 kΩ cm^2)[54]. Such small resistance at the interface between electrode surface and electrolyte proves fast electron transfer to the solution redox species and indicates that electrode kinetics is extremely sensitive to both: the electrode active surface and the boron content.

The *CPE* element is characterized by impedance $Z = Q^{-1}(i\omega)^{-n}$, where ω angular frequency, Q is *CPE* parameter and n is exponential, here in the range of 0.86 - 0.98). In this particular case, a constant phase element fulfills its role because the electrode surface is not flat but nanostructured, as it was presented in the SEM images and frequency dispersion arises[55]. The capacitance value for B:CNW electrode material was found to be 1.6×10^{-4} Ω^{-1} cm^{-2} s^n that

is one order of magnitude higher comparing to that determined for CNW and GC (c.a. 10^{-5} Ω^{-1} cm^{-2} s^{n}). The increased double layer capacitance could be related with the high contribution of sp^2 bonded carbon[56] proved by Raman spectroscopy and XPS measurement, enhanced electroactive surface area A_{eff} and according to Granger *et al.*[3] may result also from some surface charge involving surface species and higher internal charge carrier concentration affected by boron doping.

Basing on the value of charge transfer resistance and taking into account the following relation $k^\circ = RT/n^2F^2AC_{ct}$ the standard rate constant could be determined[14]. Knowing that R is the molar gas constant (8.32 J $mol^{-1}K^{-1}$), T is the electrolyte temperature (296 K), n is the number of exchanged electrons (n = 1), F is the Faraday constant (96500 C), A is attributed to the geometric electrode area (0.1256 cm^2) and $C_{ox} = C_{red} = 5\times10^{-6}$ mol cm^{-3}, the value of k° equals 1.1×10^{-2} cm/s. This value is higher compared to the glassy carbon (9.9×10^{-4} cm/s) or non-doped CNW (3.7×10^{-3} cm/s) and could be assigned to the enhanced electrochemical reactivity or as proposed by Krivenko *et al.*[20], may result from the different mechanism of redox process performed at B:CNW surface comparing to other carbon electrode materials. Nevertheless, it should be also taken into account that for the electrodes based on complex-shape morphology, the constant rate of electron transfer could be only treated as estimated value. Such caution should be considered because the conditions of redox reaction on such surfaces are far from idealized assumptions that state as a basis for the mathematical models of cyclic voltammetry.

2.3. Enhanced detection of guanine and adenine at bare B:CNWs

The "as-grown" B:CNW electrodes have been applied for the simultaneous detection of DNA purine bases: adenine and guanine by means of cyclic voltammetry and differential pulse voltammetry. The CV were obtained for a mixture of guanine and adenine in concentration

decreasing from 0.5 mM to 0.5 μM in solution of 0.1 M phosphate buffer (pH 7.0), using an 8-mm-diameter (0.5024 cm^2) of boron-doped carbon nanowalls electrode (**Figure 7A**).

The PBS buffer was chosen as supporting electrolyte for several reasons: it is close to the physiological pH, and the peaks of oxidation are separated[57–60]. The oxidation of guanine and adenine results in the well-defined oxidation peaks at positive potentials of about +0.85 and +1.17 V, respectively. The B:CNW electrode reactions are highly irreversible for both DNA bases, similarly to the case of BDD electrode[17].

Next, **Figure 7C** shows the DPV curves recorded simultaneously for the mixture of adenine and guanine in the range of concentrations extending from 0.5 mM to 0.5 μM diluted in 0.1 M phosphate buffer (pH 7.0). Both purine bases show sharp separated peaks in DPV. The peak at +0.73 V to +0.75 V is attributed to the oxidation of guanine, while +1.0 V to +1.08 V maximum results from adenine[61]. The mechanism of oxidation of both DNA purine bases is described by[62,63].

The both voltammetric experiments (CV and DPV) show that the oxidation current peak intensity versus concentration of guanine (red squares) and adenine (blue circles) displays two different linear responses: (I) at lower and (II) and higher concentration range (see **Figure 7B-D**). It is worth noting that recorded currents densities are up to one order of magnitude higher than those registered by other reported electrode systems like bare BDD[17], modified graphene[18] or electrochemically pre-treated GC[64] (see **Table 3 and 4**), what is attributed to the enhanced charge transfer in B:CNW material related with decreased double layer capacitance.

Table 3. The linear regression equations and determination coefficient (R^2) of adenine (A) and guanine (G) recorded by cyclic voltamperometry and differential pulse voltammetry.

	Purine	**Linear regression equation**	**R^2**
	A (I)	I_{pa} (μA) = 1.7210 C + 35.4444 (μM)	0.935

CV	**G (I)**	I_{pa} (μA) = 2.4815 C + 13.5093 (μM)	0.925
	A (II)	I_{pa} (μA) = 0.7762 C + 50.8841 (μM)	0.999
	G (II)	I_{pa} (μA) = 0.4595 C + 47.5767 (μM)	0.992
DPV	**A (I)**	I_{pa} (μA) = 1.7548 C + 29.7157 (μM)	0.945
	G (I)	I_{pa} (μA) = 2.1140 C + 16.8594 (μM)	0.959
	A (II)	I_{pa} (μA) = 0.1130 C + 40.9162 (μM)	0.966
	G (II)	I_{pa} (μA) = 0.1097 C + 42.0832 (μM)	0.988

Table 3 lists the linear regression equations I_{pa} and the correlation coefficients R^2 versus specific conditions and concentration range. The lower ranges (I): (CV: 15 μM to 1 μM) and (DPV: 8 μM - 0.5 μM) slopes are significantly greater than those estimated in the higher concentration ranges (II) (see **Table 3** and **Figure 7B-D**). This phenomenon demonstrates fitting to Langmuir adsorption isotherm behavior[65] and it could originates from the formation of a monolayer of adsorbed guanine at the electrode surface at low concentration ranges[61].

Table 4. The comparison of sensitivities of various electrodes towards simultaneous detection of guanine and adenine.

	Electrode	**Slope nA μM^{-1}**	**Sensitivity μA μM^{-1} cm^{-2}**	**Linear Range μM**	**LOD μM**	**Reference**
Guanine	BDD	8	0.1132	0.3–19	0.158	[17]
	graphene-COOH	7.5	0.1061	0.5–200	0.05	[18]
	pre-treated GC	34.46	1.95	0.2–10	0.06	[61]
	glassy carbon	50	0.7074	(5-50) and (50-230)	0.5	[66]
	B-CNTs	300	4.2441	2.5–18	0.5	[67]
	carbon fibers @GC	900	12.7324	0.50 to 12.0	0.01	[68]
	B:CNW	2114	4.2057	(0.5-8) and (50-500)	1.36	This work
Adenine	BDD	9	0.1273	0.3–19	0.067	[17]
	graphene-COOH	6.5	0.092	0.5–200	0.025	[18]
	pre-treated GC	33.67	1.9053	0.2–10	0.07	[61]
	glassy carbon	34	0.481	(20-70) and (70-230)	0.5	[66]
	B-CNTs	200	2.8294	3.5-20	0.48	[67]
	carbon fibers @GC	unlinear	unlinear	0.5 - 8	0.03	[68]
	B:CNW	1754.8	3.4911	(0.5-8) and (50-500)	1.6	This work

For comparative evaluation, the analytical performance for simultaneous detection of G and A on bare B:CNW and other referenced nanomaterials are listed in **Table 4**. The limit of detection (LOD) of adenine (according to a signal-to-noise ratio of 3) is estimated to 1.6 μM, while guanine studies effects in 1.36 μM of LOD. Both limits were achieved using DPV technique. Overall, **Table 4** shows that B:CNW results in competitive sensitivity and current efficiency. The size of the electrode could be easily scaled-up keeping physical homogeneity and electrochemical performance. The values shown above and the shape of DPV curves originate from the properties of (B:CNW) electrode, which possess a very developed surface and enhanced current densities. The low concentrations of analytes causes that the outer, more accessible active surface area could be fully covered with a lower competition for the surface. It ensures a more efficient uptake and adsorption of adenine, and guanine leading to a higher sensitivity for the lower concentrations. This phenomenon has been also observed previously for the simultaneous determination of adenine and guanine using GC electrode modified by polypyrrole/graphene[69].

The experiments were done three times for detection of adenine and guanine on separately deposited B-CNW electrodes. Three freshly prepared electrodes were used for the detection of G and A. The replicate measurements of a 10 μ M mixture solution of G and A resulted in the avg. RSD value of 1.43 %, while three parallel grown electrodes were used to determine 10 μ M mixture solution of G and A with avg. RSD value of 2.6 %, showing satisfactory reproducibility.

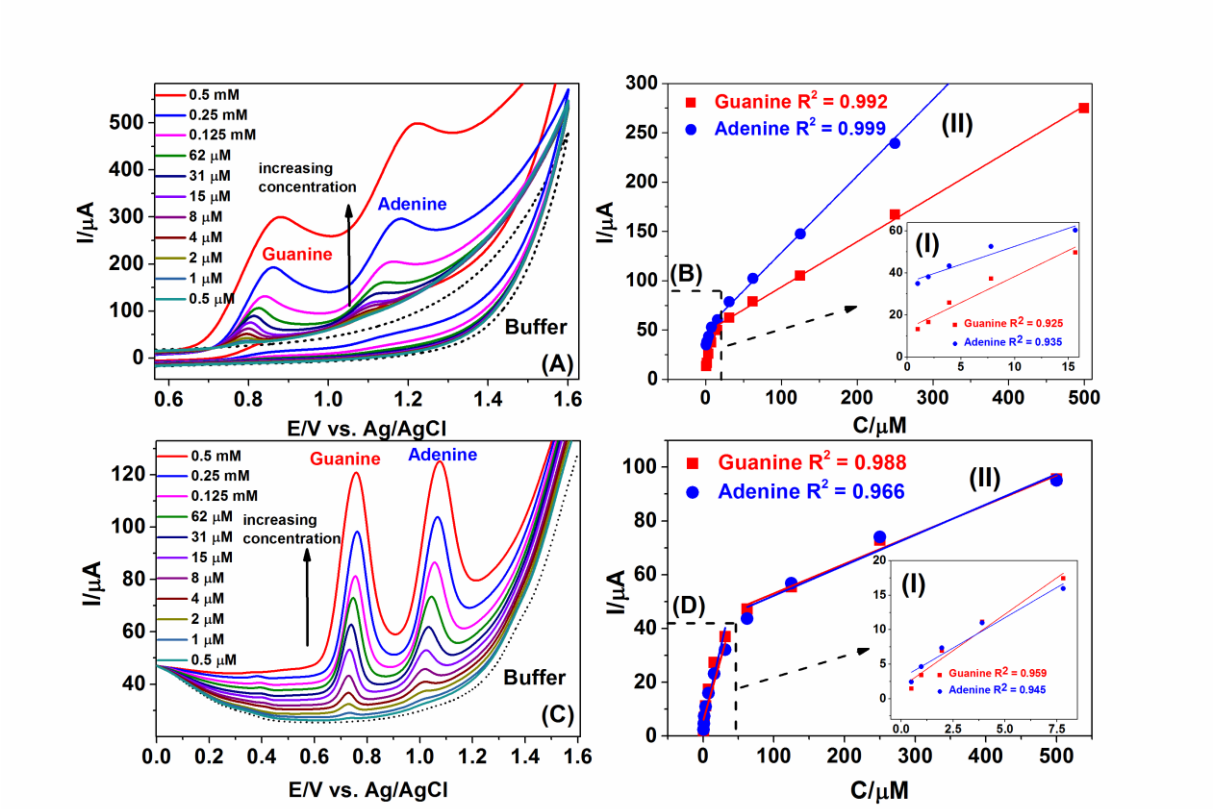

Figure 7. The cyclic voltammograms (A) and differential pulse voltammograms (C) of the simultaneous determination of guanine and adenine in 0.1 M phosphate buffer solutions (pH 7.0) containing concentration from 0.5 mM to 0.1 μM. The plots (B) and (D) present the peak currents as a function of concentration of guanine and adenine.

Next, the experiments comparing the sensitivities of B:CNW and CNW electrodes towards the simultaneous oxidation of guanine and adenine show an obvious improvement of carbon nanowalls by boron doping (see **Figure 8**). The CV and DPV curves of B:CNW electrode registered during guanine and adenine oxidation, presented in **Figure 8**, exhibit the current efficiency of above one order of magnitude higher when compared with that recorded for undoped CNWs. This fact implies much lower sensitivity and limit of detection, when no doping was applied.

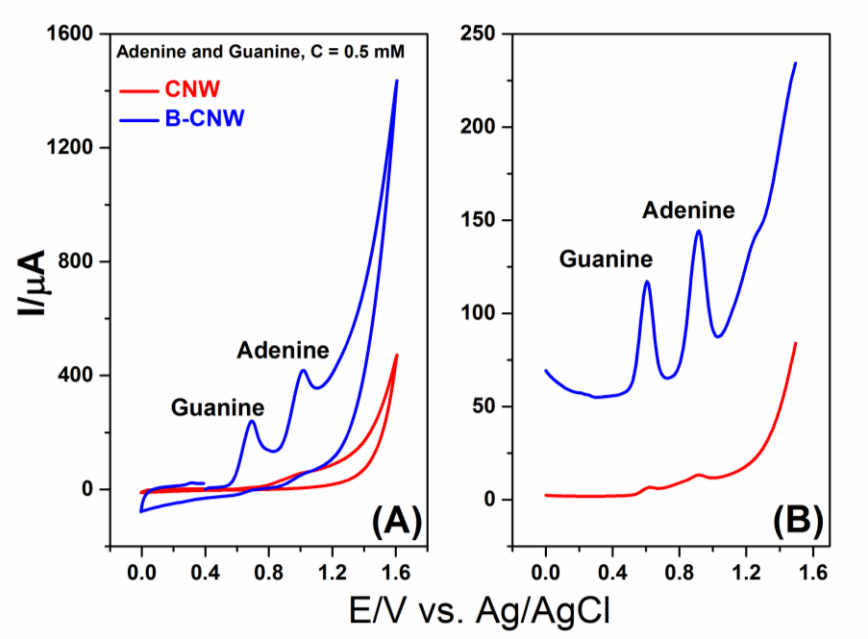

Figure 8. The cyclic voltammograms (A) and differential pulse voltammograms (B) of the simultaneous determination of guanine and adenine in 0.1 M phosphate buffer solutions (pH 7.0) in concentration 0.5 mM of each purine base. Undoped CNW electrode has been shown for direct comparison of current efficiency and implied decreased detection sensitivity.

It is obvious that B:CNWs provided slightly higher LODs but then higher sensitivities when compared with similar geometrical sizes of surfaces of working electrodes e.g. pre-treated glassy carbon[64] or boron-doped diamond[17] (see **Table 4**). Nevertheless, it should be clearly stated that B:CNW is a low-cost, carbon-based material allowing for the simultaneous determination of G and A without need of further modification or pre-treatment.

The extended voltammetric studies on the B:CNW selectivity towards detection of adenine, guanine, thymine and cytosine have also been carried out (see Figure S3 in ESI). The DPV results reveal that simultaneous detection of four purine bases (A, G, T and C) could be achieved at B:CNW electrodes as illustrated in Figure S3A. Next, the separated detection of T and C, shown in Figure S3B (given in ESI), led to detection of sensitivity of thymine and cytosine of approx. 62 μM and 1.25 mM respectively. The further detailed studies on the boron

level doping in the B:CNW and surface modification improving C and T oxidation mediation is in progress. The B:CNW electrodes were also applied to investigate the DPV curves of calf thymus DNA sequences in concentration of 0.125 mM, and the corresponding results are shown in **Figure S4** (given in ESI). The peaks of guanine, adenine and cytosine occur in oxidation process of DNA. This demonstrates that the B:CNW electrodes have potential for application in the analysis of DNA. Last but not least, the detection processes here generate higher current densities than those registered by other reported electrode systems. It allows for the application of B:CNWs in low-cost read-out electronic systems or low-power point-of-care handheld devices.

3. Conclusions

Summarizing, the effective synthesis of novel B:CNW was shown without additional substrate pretreatment or usage of multi-step plasma growth. Fabricated samples consist of sharp edged, flat and up to 3 μm long carbon walls. The B:CNW shows high boron doping concentration of 1.3% at. and low nitrogen incorporation of 0.4% at. It should be noted that samples showing outstanding electrochemical performance, followed by high rate k° equals 1.1×10^{-2} cm/s and ΔE as 85 mV much lower in comparison to the glassy carbon or undoped carbon nanowalls. This material can be strongly considered as high kinetic electrode in biosensing or energy storage applications. The obtained results directly indicated that novel material called boron-doped carbon nanowalls (B:CNW) have excellent electrocatalytic activity towards the oxidation of guanine and adenine simultaneously without additional functionalization. It is worth noting that recorded currents are higher than those registered by other electrodes i.e. BDD, graphene or GC. Nonetheless, it can be stated that the bare B:CNW electrode is a highly sensitive electrochemical transducer for the simultaneous detection of G and A.

4. Experimental Section

Electrode growth: B:CNW were synthesized using the MW PE CVD system (SEKI Technotron AX5400S, Japan). The base pressure inside the chamber was 10^{-4} Torr. Several B:CNW films were fabricated using the following process conditions: Gas mixtures — H_2, CH_4, B_2H_6 and N_2 with total flow 328 sccm, process pressure 50 Torr, microwave power — up to 1.3 kW, microwave radiation 2.45 GHz and growth time of up to 6 hours. During the process, the substrate holder was heated up to 700°C by an induction heater, which was controlled by a thermocouple. B:CNW thin films were grown on (100) oriented silicon substrates. Before the CVD growth, Si substrates were seeded by spin-coating in the diamond slurry yielding high seeding densities in the range up to 10^{10} cm^{-2}.

Surface Morphology: Scanning Electron Microscope FEI Quanta FEG 250 Scanning Electron Microscope (SEM) using 10kV beam accelerating voltage with SE-ETD detector (secondary electron - Everhart-Thornley detector) working in high vacuum mode (pressure 10^{-4} Pa) was used to observed the structure of the surface of B:CNW. The morphology studies were performed with optical microscopy using combination with a 20x objective magnification and numerical aperture 0.4 and program for data visualization and analysis (Gwyddion, 2.40, Czech Republic).

Chemical Composition: The chemical composition of the deposited films was studied by means of Raman spectroscopy using Raman confocal microscope (Horiba LabRAM ARAMIS, Japan). Spectra were recorded in a range of 200–3500 cm^{-1} with an integration time of 5 s (10 averages), using a 532 nm diode pumped solid state (DPSS) laser in combination with a 50 × objective magnification (NA = 0.5) and a 50 μm confocal aperture. The Lorentzian function has been

applied to deconvolute peaks recorded in the B:NCD Raman spectrum (OriginPro 8.0, OriginLab, Northampton, MA).

X-Ray Photoelectron Spectroscopy: (XPS) analysis was performed with Escalab 250Xi (ThermoFisher Scientific, United Kingdom) equipped in monochromatic Al X-Ray source. High resolution spectra were made at a pass energy of 10 eV, and energy step size of 0.1 eV. X-ray spot size was 650 μm. In order to normalize the spectroscopic measurements, the X axis (binding energy) from XPS spectrum was calibrated for peak characteristics of neutral carbon C1s (284.6 eV).

*Electrochemical evaluation***:** Electrochemical measurements composite electrodes were performed by the potentionstat-galvanostat system AutoLab PGStat 302N in a standard three-electrode assembly at 295 K. The Si substrate covered with B:CNW stayed as a working electrode. As reference samples non-doped carbon nanowalls (CNW) and glassy carbon (GC, 2 mm in diameter) were used. For electrochemical studies, the specimen holder made from Polyether ether ketone material was fabricated. It enables contact between limited electrode surface and electrolyte. The diameter of round sample area wetted by electrolyte was 4 mm. All current densities in this manuscript were calculated on the basis of the geometric surface area. Before measurements, working electrode was not treated electrochemically in any way. The counter electrode consisted of Pt gauze and reference electrode: Ag/AgCl/3 M KCl. Electrodes were tested by cyclic voltammetry in solutions: 0.5 M K_2SO_4 without and with 5 mM $K_3Fe(CN)_6$ or 5 mM of hydroquinone (HQ) as a redox probe (**Figure S1** and **Table S1** given in ESI). Electrochemical impedance spectroscopy measurement for each electrode material immersed in $K_3Fe(CN)_6$ solution was carried out at the determined formal redox potential in the frequency range of 0.1 Hz to 20 kHz and amplitude 10 mV. All electrolytes used were

purged with argon for 50 min. before the electrochemical test and during measurements there was an Ar-cushion above the electrolyte.

The impedance data were analyzed on the basis of an electric equivalent circuit (*EEQC*) using an EIS Spectrum Analyser. The modified Powell algorithm[70] was used with amplitude weighting r_a:

$$r_a = (\omega, P_1 ... P_M) = r_c^2 / (N - M),$$

where N is the number of points, M is the number of parameters, ω is the angular frequency, $P_1 ... P_M$ are parameters. Parameter r_c is defined as:

$$r_c^2 = \sum_{i=1}^{N} \frac{\left(Z_i^{'} - Z_{i_{calc}}^{'}\right)^2 + \left(Z_i^{''} - Z_{i_{calc}}^{''}\right)^2}{Z_i^{'2} + Z_{i_{calc}}^{'\ 2}},$$

where i corresponds to the measured values of impedance and i_{calc} is attributed to the calculated values; N is the number of points.

Moreover, guanine and adenine were obtained from Sigma-Aldrich and used without further purification. The boron-doped carbon nanowalls working electrode (B:CNW, disk diameter 8.0 mm, surface area ca. 0.5 cm^2) was applied in detection studies. Voltammetric measurements were performed by a potentiostat-galvanostat. The experimental conditions were: cyclic voltammetry (CV), the potential ranging from 0 to 1.6 V, scan rate 100 mV/s; differential pulse voltammetry (DPV), the same potential range like in CV, amplitude modulation of 50 mV, pulse width of 70 ms, and a scan rate of 5 mV/s. The CV and DPV measurements were performed in 0.1 M PBS (pH = 7.0) with different concentrations of adenine or guanine or their mixtures.

Supporting Information. The comparison of cyclic voltammetry curves registered for GC, CNW and B:CNW electrodes and differential pulsed voltammetry determination of thymine, cytosine and calf thymus DNA.

Acknowledgements

The authors gratefully acknowledge financial support from the Polish National Science Centre (NCN) under Grant No. 2012/07/D/ST5/02269, 2015/17/D/ST5/02571 and 2014/14/M/ST5/00715. The DS funds of the Faculty of Electronics, Telecommunications and Informatics of the Gdansk University of Technology are also acknowledged. K. S. research was supported by the Foundation for Polish Science (FNP).

References

(1) Cha, C.; Shin, S. R.; Annabi, N.; Dokmeci, M. R.; Khademhosseini, A. Carbon-Based Nanomaterials: Multifunctional Materials for Biomedical Engineering. *ACS Nano* **2013**, *7* (4), 2891–2897.

(2) Iijima, S.; Ichihashi, T. Single-Shell Carbon Nanotubes of 1-Nm Diameter. *Nature* **1993**, *363* (6430), 603–605.

(3) Granger, M. C.; Swain, G. M. The Influence of Surface Interactions on the Reversibility of Ferri/Ferrocyanide at Boron-Doped Diamond Thin-Film Electrodes. *J. Electrochem. Soc.* **1999**, *146* (12), 4551–4558.

(4) Patil, A. J.; Vickery, J. L.; Scott, T. B.; Mann, S. Aqueous Stabilization and Self-Assembly of Graphene Sheets into Layered Bio-Nanocomposites Using DNA. *Adv. Mater.* **2009**, *21* (31), 3159–3164.

(5) Shang, N. G.; Au, F. C. K.; Meng, X. M.; Lee, C. S.; Bello, I.; Lee, S. T. Uniform Carbon Nanoflake Films and Their Field Emissions. *Chem. Phys. Lett.* **2002**, *358* (3–4), 187–191.

(6) Wang, J.; Zhu, M.; Outlaw, R. A.; Zhao, X.; Manos, D. M.; Holloway, B. C. Synthesis of Carbon Nanosheets by Inductively Coupled Radio-Frequency Plasma Enhanced Chemical Vapor Deposition. *Carbon* **2004**, *42* (14), 2867–2872.

(7) Wu, Y.; Qiao, P.; Chong, T.; Shen, Z. Carbon Nanowalls Grown by Microwave Plasma Enhanced Chemical Vapor Deposition. *Adv. Mater.* **2002**, *14* (1), 64–67.

(8) Hiramatsu, M.; Shiji, K.; Amano, H.; Hori, M. Fabrication of Vertically Aligned Carbon Nanowalls Using Capacitively Coupled Plasma-Enhanced Chemical Vapor Deposition Assisted by Hydrogen Radical Injection. *Appl. Phys. Lett.* **2004**, *84* (23), 4708.

(9) Hiramatsu, M.; Hori, M. *Carbon Nanowalls: Synthesis and Emerging Applications*, 2010 edition.; Springer, 2010.

(10) Zhu, S.; Li, J.; Li, Q.; He, C.; Liu, E.; He, F.; Shi, C.; Zhao, N. Space-Confined Synthesis of Three-Dimensional Boron/Nitrogen-Doped Carbon Nanotubes/Carbon Nanosheets Line-in-Wall Hybrids and Their Electrochemical Energy Storage Applications. *Electrochim. Acta* **2016**, *212*, 621–629.
(11) Lu, C.; Dong, Q.; Tulugan, K.; Park, Y. M.; More, M. A.; Kim, J.; Kim, T. G. Characteristic Study of Boron Doped Carbon Nanowalls Films Deposited by Microwave Plasma Enhanced Chemical Vapor Deposition. *J. Nanosci. Nanotechnol.* **2016**, *16* (2), 1680–1684.
(12) Kurita, S.; Yoshimura, A.; Kawamoto, H.; Uchida, T.; Kojima, K.; Tachibana, M.; Molina-Morales, P.; Nakai, H. Raman Spectra of Carbon Nanowalls Grown by Plasma-Enhanced Chemical Vapor Deposition. *J. Appl. Phys.* **2005**, *97* (10), 104320.
(13) Yang, J.; Chen, J.; Yu, S.; Yan, X.; Xue, Q. Synthesis of a Graphene Nanosheet Film with Attached Amorphous Carbon Nanoparticles by Their Simultaneous Electrodeposition. *Carbon* **2010**, *48* (9), 2665–2668.
(14) Luais, E.; Boujtita, M.; Gohier, A.; Tailleur, A.; Casimirius, S.; Djouadi, M. A.; Granier, A.; Tessier, P. Y. Carbon Nanowalls as Material for Electrochemical Transducers. *Appl. Phys. Lett.* **2009**, *95* (1), 14104.
(15) Granger, M. C.; Witek, M.; Xu, J.; Wang, J.; Hupert, M.; Hanks, A.; Koppang, M. D.; Butler, J. E.; Lucazeau, G.; Mermoux, M.; Strojek, J. W.; Swain, G. M. Standard Electrochemical Behavior of High-Quality, Boron-Doped Polycrystalline Diamond Thin-Film Electrodes. *Anal. Chem.* **2000**, *72* (16), 3793–3804.
(16) Wang, H.-S.; Ju, H.-X.; Chen, H.-Y. Simultaneous Determination of Guanine and Adenine in DNA Using an Electrochemically Pretreated Glassy Carbon Electrode. *Anal. Chim. Acta* **2002**, *461* (2), 243–250.
(17) Švorc, Ľ.; Kalcher, K. Modification-Free Electrochemical Approach for Sensitive Monitoring of Purine DNA Bases: Simultaneous Determination of Guanine and Adenine in Biological Samples Using Boron-Doped Diamond Electrode. *Sens. Actuators B Chem.* **2014**, *194*, 332–342.
(18) Huang, K.-J.; Niu, D.-J.; Sun, J.-Y.; Han, C.-H.; Wu, Z.-W.; Li, Y.-L.; Xiong, X.-Q. Novel Electrochemical Sensor Based on Functionalized Graphene for Simultaneous Determination of Adenine and Guanine in DNA. *Colloids Surf. B Biointerfaces* **2011**, *82* (2), 543–549.
(19) Yin, H.; Zhou, Y.; Ma, Q.; Ai, S.; Ju, P.; Zhu, L.; Lu, L. Electrochemical Oxidation Behavior of Guanine and Adenine on graphene–Nafion Composite Film Modified Glassy Carbon Electrode and the Simultaneous Determination. *Process Biochem.* **2010**, *45* (10), 1707–1712.
(20) Krivenko, A. G.; Komarova, N. S.; Stenina, E. V.; Sviridova, L. N.; Mironovich, K. V.; Shul'ga, Y. M.; Manzhos, R. A.; Doronin, S. V.; Krivchenko, V. A. Electrochemical Modification of Electrodes Based on Highly Oriented Carbon Nanowalls. *Russ. J. Electrochem.* **2015**, *51* (10), 963–975.
(21) Ficek, M.; Sankaran, K. J.; Ryl, J.; Bogdanowicz, R.; Lin, I.-N.; Haenen, K.; Darowicki, K. Ellipsometric Investigation of Nitrogen Doped Diamond Thin Films Grown in Microwave CH4/H2/N2 Plasma Enhanced Chemical Vapor Deposition. *Appl. Phys. Lett.* **2016**, *108* (24), 241906.
(22) Wu, Y.; Yang, B.; Zong, B.; Sun, H.; Shen, Z.; Feng, Y. Carbon Nanowalls and Related Materials. *J. Mater. Chem.* **2004**, *14* (4), 469–477.
(23) Sen, U. K.; Mitra, S. High-Rate and High-Energy-Density Lithium-Ion Battery Anode Containing 2D MoS2 Nanowall and Cellulose Binder. *ACS Appl. Mater. Interfaces* **2013**, *5* (4), 1240–1247.

(24) Varghese, B.; Reddy, M. V.; Yanwu, Z.; Lit, C. S.; Hoong, T. C.; Subba Rao, G. V.; Chowdari, B. V. R.; Wee, A. T. S.; Lim, C. T.; Sow, C.-H. Fabrication of NiO Nanowall Electrodes for High Performance Lithium Ion Battery. *Chem. Mater.* **2008**, *20* (10), 3360–3367.
(25) BenMoussa, B.; D'Haen, J.; Borschel, C.; Barjon, J.; Soltani, A.; Mortet, V.; Ronning, C.; D'Olieslaeger, M.; Boyen, H.-G.; K Haenen. Hexagonal Boron Nitride Nanowalls: Physical Vapour Deposition, 2D/3D Morphology and Spectroscopic Analysis. *J. Phys. Appl. Phys.* **2012**, *45* (13), 135302.
(26) Lin, Y.; Connell, J. W. Advances in 2D Boron Nitride Nanostructures: Nanosheets, Nanoribbons, Nanomeshes, and Hybrids with Graphene. *Nanoscale* **2012**, *4* (22), 6908–6939.
(27) Truscott, B. S.; Kelly, M. W.; Potter, K. J.; Ashfold, M. N. R.; Mankelevich, Y. A. Microwave Plasma-Activated Chemical Vapor Deposition of Nitrogen-Doped Diamond. II: CH4/N2/H2 Plasmas. *J. Phys. Chem. A* **2016**, *120* (43), 8537–8549.
(28) Shang, N.; Papakonstantinou, P.; Wang, P.; Zakharov, A.; Palnitkar, U.; Lin, I.-N.; Chu, M.; Stamboulis, A. Self-Assembled Growth, Microstructure, and Field-Emission High-Performance of Ultrathin Diamond Nanorods. *ACS Nano* **2009**, *3* (4), 1032–1038.
(29) Sankaran, K. J.; Kurian, J.; Chen, H. C.; Dong, C. L.; Lee, C. Y.; Tai, N. H.; Lin, I. N. Origin of a Needle-like Granular Structure for Ultrananocrystalline Diamond Films Grown in a N 2 /CH 4 Plasma. *J. Phys. Appl. Phys.* **2012**, *45* (36), 365303.
(30) Yen, H.-F.; Horng, Y.-Y.; Hu, M.-S.; Yang, W.-H.; Wen, J.-R.; Ganguly, A.; Tai, Y.; Chen, K.-H.; Chen, L.-C. Vertically Aligned Epitaxial Graphene Nanowalls with Dominated Nitrogen Doping for Superior Supercapacitors. *Carbon* **2015**, *82*, 124–134.
(31) Williams, O. A.; Nesládek, M. Growth and Properties of Nanocrystalline Diamond Films. *Phys. Status Solidi A* **2006**, *203* (13), 3375–3386.
(32) Osswald, S.; Havel, M.; Gogotsi, Y. Monitoring Oxidation of Multiwalled Carbon Nanotubes by Raman Spectroscopy. *J. Raman Spectrosc.* **2007**, *38* (6), 728–736.
(33) Davami, K.; Shaygan, M.; Kheirabi, N.; Zhao, J.; Kovalenko, D. A.; Rümmeli, M. H.; Opitz, J.; Cuniberti, G.; Lee, J.-S.; Meyyappan, M. Synthesis and Characterization of Carbon Nanowalls on Different Substrates by Radio Frequency Plasma Enhanced Chemical Vapor Deposition. *Carbon* **2014**, *72*, 372–380.
(34) Luo, Z.; Shang, J.; Lim, S.; Li, D.; Xiong, Q.; Shen, Z.; Lin, J.; Yu, T. Modulating the Electronic Structures of Graphene by Controllable Hydrogenation. *Appl. Phys. Lett.* **2010**, *97* (23), 233111.
(35) Lucchese, M. M.; Stavale, F.; Ferreira, E. H. M.; Vilani, C.; Moutinho, M. V. O.; Capaz, R. B.; Achete, C. A.; Jorio, A. Quantifying Ion-Induced Defects and Raman Relaxation Length in Graphene. *Carbon* **2010**, *48* (5), 1592–1597.
(36) Achour, A.; Vizireanu, S.; Dinescu, G.; Le Brizoual, L.; Djouadi, M.-A.; Boujtita, M. Electrochemical Anodic Oxidation of Nitrogen Doped Carbon Nanowall Films: X-Ray Photoelectron and Micro-Raman Spectroscopy Study. *Appl. Surf. Sci.* **2013**, *273*, 49–57.
(37) Ryl, J.; Burczyk, L.; Bogdanowicz, R.; Sobaszek, M.; Darowicki, K. Study on Surface Termination of Boron-Doped Diamond Electrodes under Anodic Polarization in H2SO4 by Means of Dynamic Impedance Technique. *Carbon* **2016**, *96*, 1093–1105.
(38) Titantah, J. T.; Lamoen, D. Carbon and Nitrogen 1s Energy Levels in Amorphous Carbon Nitride Systems: XPS Interpretation Using First-Principles. *Diam. Relat. Mater.* **2007**, *16* (3), 581–588.
(39) Ren, Z.-M.; Du, Y.-C.; Qiu, Y.; Wu, J.-D.; Ying, Z.-F.; Xiong, X.-X.; Li, F.-M. Carbon Nitride Films Synthesized by Combined Ion-Beam and Laser-Ablation Processing. *Phys. Rev. B* **1995**, *51* (8), 5274.

(40) Ozaki, J.; Kimura, N.; Anahara, T.; Oya, A. Preparation and Oxygen Reduction Activity of BN-Doped Carbons. *Carbon* **2007**, *45* (9), 1847–1853.
(41) Sowers, A. T.; Ward, B. L.; English, S. L.; Nemanich, R. J. Field Emission Properties of Nitrogen-Doped Diamond Films. *J. Appl. Phys.* **1999**, *86* (7), 3973–3982.
(42) Hassan, S.; Suzuki, M.; Mori, S.; El-Moneim, A. A. MnO2/carbon Nanowall Electrode for Future Energy Storage Application: Effect of Carbon Nanowall Growth Period and MnO2 Mass Loading. *RSC Adv.* **2014**, *4* (39), 20479.
(43) Giorgi, L.; Makris, T. D.; Giorgi, R.; Lisi, N.; Salernitano, E. Electrochemical Properties of Carbon Nanowalls Synthesized by HF-CVD. *Sens. Actuators B Chem.* **2007**, *126* (1), 144–152.
(44) Gosser, D. K. *Cyclic Voltammetry: Simulation And Analysis Of Reaction Mechanisms*, Includes floppy Disk edition.; Wiley-VCH: New York, N.Y., 1993.
(45) Majzlíková, P.; Sedláček, J.; Prášek, J.; Pekárek, J.; Svatoš, V.; Bannov, A. G.; Jašek, O.; Synek, P.; Eliáš, M.; Zajíčková, L.; Hubálek, J. Sensing Properties of Multiwalled Carbon Nanotubes Grown in MW Plasma Torch: Electronic and Electrochemical Behavior, Gas Sensing, Field Emission, IR Absorption. *Sensors* **2015**, *15* (2), 2644–2661.
(46) Shao, Y.; Wang, J.; Wu, H.; Liu, J.; Aksay, I. A.; Lin, Y. Graphene Based Electrochemical Sensors and Biosensors: A Review. *Electroanalysis* **2010**, *22* (10), 1027–1036.
(47) Bard, A. J.; Faulkner, L. R. *Electrochemical Methods: Fundamentals and Applications*, 2nd ed.; Wiley: New York, 2001.
(48) Angell, D. H.; Dickinson, T. The Kinetics of the Ferrous/ferric and Ferro/ferricyanide Reactions at Platinum and Gold Electrodes. *J. Electroanal. Chem. Interfacial Electrochem.* **1972**, *35* (1), 55–72.
(49) Lee, S.-K.; Song, M.-J.; Kim, J.-H.; Lim, Y.-K.; Chun, Y.-S.; Lim, D.-S. Selective Growth of Carbon Nanotubes on Boron-Doped Diamond for Electrochemical Biosensor Application. *RSC Adv* **2015**, *5* (30), 23395–23400.
(50) Shalini, J.; Sankaran, K. J.; Chen, H.-C.; Lee, C.-Y.; Tai, N.-H.; Lin, I.-N. Mediatorless N2 Incorporated Diamond Nanowire Electrode for Selective Detection of NADH at Stable Low Oxidation Potential. *Analyst* **2014**, *139* (4), 778–785.
(51) Li, W.; Zhang, Z.; Tang, Y.; Bian, H.; Ng, T.; Zhang, W.; Lee, C. Graphene-Nanowall-Decorated Carbon Felt with Excellent Electrochemical Activity Toward VO2 +/VO2+ Couple for All Vanadium Redox Flow Battery. *Adv. Sci.* **2015**, *3* (4).
(52) Shalini, J.; Sankaran, K. J.; Lee, C.-Y.; Tai, N.-H.; Lin, I.-N. An Amperometric Urea Bisosensor Based on Covalent Immobilization of Urease on N2 Incorporated Diamond Nanowire Electrode. *Biosens. Bioelectron.* **2014**, *56*, 64–70.
(53) Del Río, R.; Armijo, F.; Schrebler, R.; Del Canto, G.; Vergara, C.; Gutierrez, C. Modification of boron doped diamond electrodes with glucose oxidase, characterization by electrochemical techniques. *J. Chil. Chem. Soc.* **2011**, *56* (1), 621–624.
(54) Oliveira, S. C. B.; Oliveira-Brett, A. M. Voltammetric and Electrochemical Impedance Spectroscopy Characterization of a Cathodic and Anodic Pre-Treated Boron Doped Diamond Electrode. *Electrochim. Acta* **2010**, *55* (15), 4599–4605.
(55) Živcová, Z. V.; Petrák, V.; Frank, O.; Kavan, L. Electrochemical Impedance Spectroscopy of Polycrystalline Boron Doped Diamond Layers with Hydrogen and Oxygen Terminated Surface. *Diam. Relat. Mater.* **2015**, *55*, 70–76.
(56) Watanabe, T.; Shimizu, T. K.; Tateyama, Y.; Kim, Y.; Kawai, M.; Einaga, Y. Giant Electric Double-Layer Capacitance of Heavily Boron-Doped Diamond Electrode. *Diam. Relat. Mater.* **2010**, *19* (7–9), 772–777.

(57) Liu, H.; Wang, G.; Chen, D.; Zhang, W.; Li, C.; Fang, B. Fabrication of polythionine/NPAu/MWNTs Modified Electrode for Simultaneous Determination of Adenine and Guanine in DNA. *Sens. Actuators B Chem.* **2008**, *128* (2), 414–421.
(58) Shen, Q.; Wang, X. Simultaneous Determination of Adenine, Guanine and Thymine Based on β-cyclodextrin/MWNTs Modified Electrode. *J. Electroanal. Chem.* **2009**, *632* (1–2), 149–153.
(59) Barman, K.; Jasimuddin, S. Electrochemical Detection of Adenine and Guanine Using a Self-Assembled copper(II)–thiophenyl-Azo-Imidazole Complex Monolayer Modified Gold Electrode. *RSC Adv.* **2014**, *4* (91), 49819–49826.
(60) Arvand, M.; Motaghed Mazhabi, R.; Niazi, A. Simultaneous Determination of Guanine, Adenine and Thymine Using a Modified Carbon Paste Electrode by TiO2 Nanoparticles-magnesium(II) Doped Natrolite Zeolite. *Electrochim. Acta* **2013**, *89*, 669–679.
(61) Oliveira-Brett, A. M.; Silva, L. A. da; Brett, C. M. A. Adsorption of Guanine, Guanosine, and Adenine at Electrodes Studied by Differential Pulse Voltammetry and Electrochemical Impedance. *Langmuir* **2002**, *18* (6), 2326–2330.
(62) Li, Q.; Batchelor-McAuley, C.; Compton, R. G. Electrochemical Oxidation of Guanine: Electrode Reaction Mechanism and Tailoring Carbon Electrode Surfaces To Switch between Adsorptive and Diffusional Responses. *J. Phys. Chem. B* **2010**, *114* (21), 7423–7428.
(63) Li, J.; Jiang, J.; Feng, H.; Xu, Z.; Tang, S.; Deng, P.; Qian, D. Facile Synthesis of 3D Porous Nitrogen-Doped Graphene as an Efficient Electrocatalyst for Adenine Sensing. *RSC Adv.* **2016**, *6* (37), 31565–31573.
(64) Oliveira-Brett, A. M.; Piedade, J. A. P.; Silva, L. A.; Diculescu, V. C. Voltammetric Determination of All DNA Nucleotides. *Anal. Biochem.* **2004**, *332* (2), 321–329.
(65) Brett, C. M. A.; Brett, A. M. O. *Electrochemistry: Principles, Methods, and Applications*; Oxford science publications; Oxford University Press: Oxford ; New York, 1993.
(66) Li, H.; Wang, X.; Wang, Z.; Zhao, W. Simultaneous Determination of Guanine, Adenine, Thymine and Cytosine with a Simple Electrochemical Method. *J. Solid State Electrochem.* **2016**, *20* (8), 2223–2230.
(67) Ren, S.; Wang, H.; Zhang, H.; Yu, L.; Li, M.; Li, M. Direct Electrocatalytic and Simultaneous Determination of Purine and Pyrimidine DNA Bases Using Novel Mesoporous Carbon Fibers as Electrocatalyst. *J. Electroanal. Chem.* **2015**, *750*, 65–73.
(68) Deng, C.; Xia, Y.; Xiao, C.; Nie, Z.; Yang, M.; Si, S. Electrochemical Oxidation of Purine and Pyrimidine Bases Based on the Boron-Doped Nanotubes Modified Electrode. *Biosens. Bioelectron.* **2012**, *31* (1), 469–474.
(69) Gao, Y.-S.; Xu, J.-K.; Lu, L.-M.; Wu, L.-P.; Zhang, K.-X.; Nie, T.; Zhu, X.-F.; Wu, Y. Overoxidized Polypyrrole/graphene Nanocomposite with Good Electrochemical Performance as Novel Electrode Material for the Detection of Adenine and Guanine. *Biosens. Bioelectron.* **2014**, *62*, 261–267.
(70) Lu, L.; Brown, B. H.; Barber, D. C.; Leathard, A. D. A Fast Parametric Modelling Algorithm with the Powell Method. *Physiol. Meas.* **1995**, *16* (3A), A39.

Supporting Information

Boron enhanced growth of micron-length carbon based nanowalls: A route towards high rates electrochemical biosensing

*Katarzyna Siuzdak[1], Mateusz Ficek[2], Michał Sobaszek[2], Jacek Ryl[3], Marcin Gnyba[2], Paweł Niedziałkowski[4], Natalia Malinowska[4], Jakub Karczewski[5] and Robert Bogdanowicz[2]**

[1] Centre for Plasma and Laser Engineering, The Szewalski Institute of Fluid-Flow Machinery, Polish Academy of Sciences, 14 Fiszera St., 80-231 Gdansk, Poland

[2] Department of Metrology and Optoelectronics, Faculty of Electronics, Telecommunications and Informatics, Gdansk University of Technology, 11/12 G. Narutowicza St., 80-233 Gdansk, Poland

[3] Department of Electrochemistry, Corrosion and Materials Engineering, Faculty of Chemistry, Gdansk University of Technology, 11/12 Narutowicza St., 80-233 Gdansk, Poland

[4] Department of Analytical Chemistry, Faculty of Chemistry, University of Gdansk, 63 Wita Stwosza St., 80-952 Gdansk, Poland

[5] Faculty of Applied Physics and Mathematics, Gdansk University of Technology, 11/12 G. Narutowicza St., 80-233 Gdansk, Poland

***Corresponding author:** E-mail: rbogdan@eti.pg.gda.pl (Robert Bogdanowicz); Tel.: +48-58-347-15-03; Fax: +48 58-347-18-48

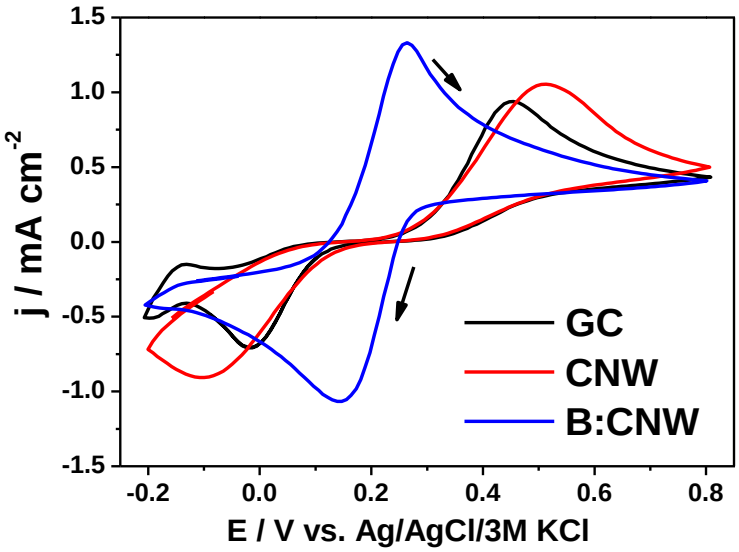

Fig. S1. The cyclic voltammetry curves registered for GC, CNW and B:CNW electrodes immersed in 5 mM HQ + 0.5 M K_2SO_4.

Table S1. The values of oxidation (E_{ox}) and reduction potentials (E_{red}) together with the separation peak value (ΔE) obtained from CV curves shown in **Fig. S1**.

sample	E_{ox} / mV	E_{red} / mV	ΔE / mV
B:CNW	265	142	123
CNW	514	-103	617
GC	451	-16	467

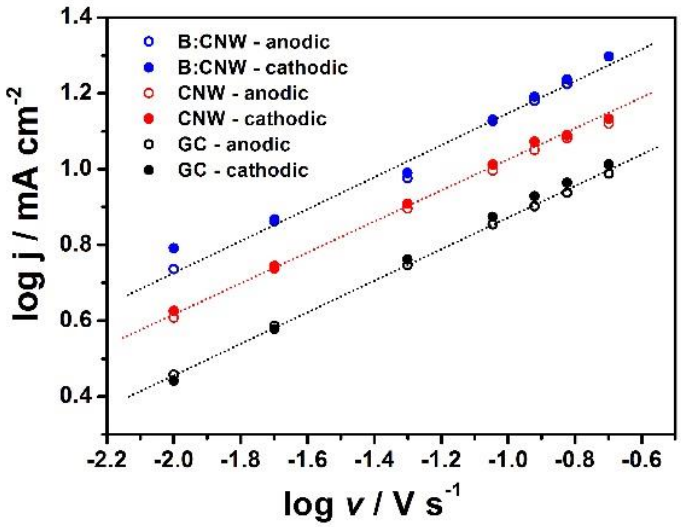

Fig. S2. The relation of logarithm of current density versus the logarithm of the scan rate obtained on the basis of Fig. 5.

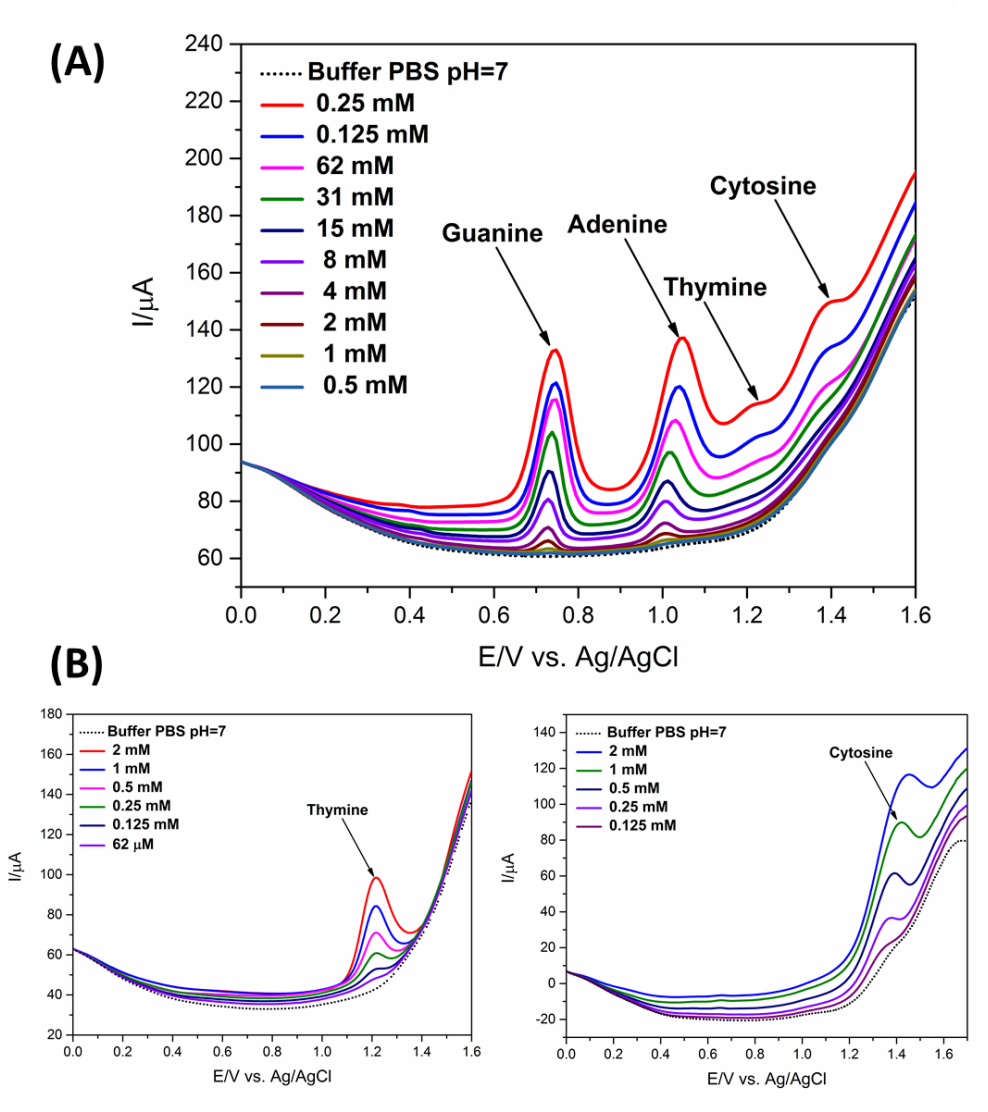

Figure S3. The differential pulse voltammograms of the simultaneous (A) determination of adenine, guanine, thymine and cytosine and separated (B) studies of thymine and cytosine, both in 0.1 M phosphate buffer solutions (pH 7.0) containing various concentrations of purine bases.

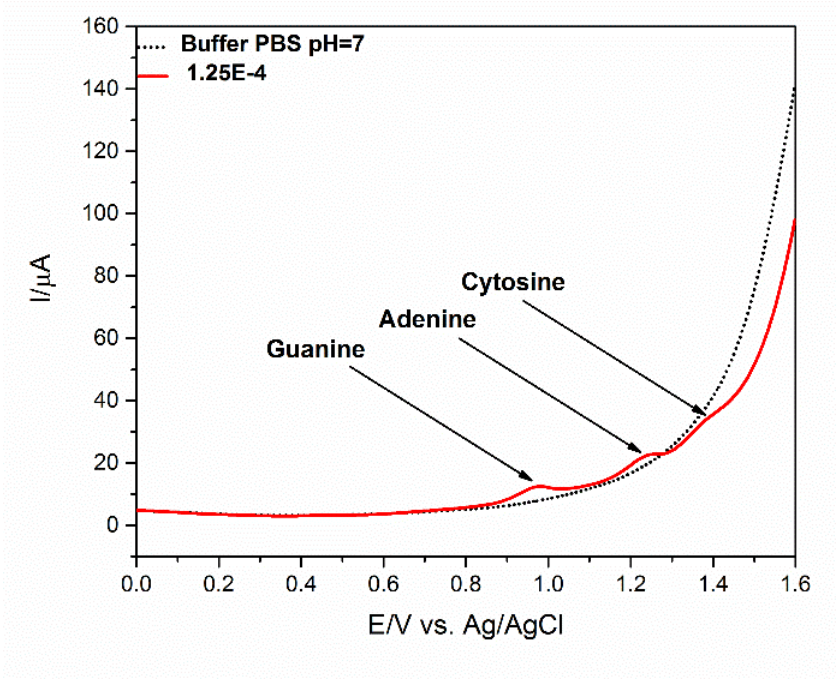

Figure S4. The detection of calf thymus DNA (CT-DNA) using DPV method in concentration 0.125 mM of DNA.